Electronic Supplementary Material (ESI) for Journal of Materials Chemistry C.

Supporting Information

Inducing formation of a corrugated, white-light emitting 2D lead-bromide perovskite via subtle changes in templating cation

Benny Febriansyah,[a,b,c] *David Giovanni,*[d] *Ramesh Sankaran,*[c,d] *Teck Ming Koh,*[b] *Yongxin Li,*[a] *Tze Chien Sum,*[d] *Nripan Mathews,*[b,e] *and Jason England*[a*]

[a]Division of Chemistry and Biological Chemistry, School of Physical and Mathematical Sciences, Nanyang Technological University, 21 Nanyang Link, Singapore 637371, Singapore.

[b]Energy Research Institute at Nanyang Technological University (ERI@N), Research Techno Plaza, X-Frontier Block Level 5, 50 Nanyang Drive, Singapore 637553, Singapore.

[c]Interdiscipinary Graduate School (IGS), Nanyang Technological University, 50 Nanyang Avenue, Singapore 639798, Singapore.

[d]Division of Physics and Applied Physics, School of Physical and Mathematical Sciences, Nanyang Technological University, 21 Nanyang Link, Singapore 637371, Singapore.

[e]School of Materials Science and Engineering, Nanyang Technological University, 50 Nanyang Avenue, Singapore 639798, Singapore.

Materials Synthesis

Chemicals. Aqueous hydrobromic acid, lead(II) bromide, 2-(4*H*-imidazol-4-yl)ethan-1-amine, 2-(pyridin-3-yl)ethan-1-amine, 2-(pyridin-4-yl)ethan-1-amine, 2-(1*H*-Imidazol-1-yl)ethanamine and 2-(2H-imidazol-2-yl)ethan-1-amine were purchased from commercial vendors. Unless otherwise stated, all reagents were used without purification.

General procedure for preparation of the ammonium bromide salts. To a round bottom flask containing an ethanolic solution of the requisite amine, cooled to 0°C, a stoichiometric amount of concentrated hydrobromic acid was added. After stirring the solution for 1 hour, all volatiles were removed using a rotary evaporator. The solids, thereby, obtained were washed with copious amounts of diethyl ether and dried under vacuum, at 50°C, overnight.

Preparation of hybrid perovskites. In general, mixtures of stoichiometric amounts of $PbBr_2$ and organic bromide salt were added to a round bottom flask containing concentrated aqueous HBr (to give concentrations of Pb^{2+} of 0.25 – 0.30 M) and heated, with stirring, at ~120°C for around 1 h. The clear solutions that resulted were allowed to cool *slowly* to room temperature, which afforded single crystals suitable for X-ray crystallography.

Thin film fabrication. Thin films used for UV-vis absorbance characterization purposes were prepared as follows: 0.50 M solutions of stoichiometric amounts of the respective 2D perovskites, dissolved in DMSO, were spin coated onto pre-cleaned glass substrates (cleaned by sequential 15 minute sonication in soap solution (Decon), deionized water, ethanol, and acetone, followed by ozone plasma treatment for 15 mins), at 3000 rpm for 30 s. The resulting films were, subsequently, heated at 110°C for 10mins.

Instrumentation and Methods

UV-Vis spectroscopy. UV-vis absorption spectra of the thin films samples were recorded using a SHIMADZU UV-3600 spectrophotometer, with an integrating sphere (ISR-3100), in the wavelength range 300 – 800 nm and a scanning resolution of 0.5 nm s^{-1}.

Steady-state, time-resolved, temperature- and power-dependent photoluminescence (PL) spectroscopies. Samples were photoexcited using 325 nm femtosecond laser pulses, generated with an optical parametric amplifier (OPA, Coherent OPerA Solo). The OPA was powered by using Coherent LIBRA laser, with a fundamental wavelength of 800 nm and output pulse-width of ~50 fs, at a repetition rate of 1 kHz. The PL signal was collected using a lens pair and sent to a spectrometer (Princeton Instrument, SP-2500 series), where it was detected in steady-state and TRPL measurements by a CCD (Pixis-400) and streak camera (Optronis), respectively. The power-dependent measurements were obtained in this configuration using a set of variable density filters to change the excitation fluence in the range of *ca.* 5 – 50 μJ/cm^2. For temperature-dependent measurements, the samples were mounted onto a liquid nitrogen-cooled Janis st-300 cryostat, adjusted to the optical plane of the inverted microscope, and measured within the temperature range 77 – 293 K.

X-ray single crystallography. Crystals were mounted on a Bruker X8 Quest CPAD area detector diffractometer and data was collected using a IμS 3.0 Microfocus Mo-Kα radiation (λ = 0.71073Å), at cryogenic temperatures (100K). Data reduction and absorption corrections were performed using the SAINT and SADABS software packages, respectively.[1] All structures were solved by direct methods and refined by full-matrix least squares procedures on F^2, using the Bruker SHELXTL-2014 software package.[2,3] Non-hydrogen atoms were anisotropically refined, after which hydrogen atoms were introduced at calculated positions and further refinement of data was performed. Graphical depictions of the crystal structures used throughout the manuscript were created using the program VESTA.[4]

Analysis of structural distortions in 2D perovskites. Distortions of the $[PbBr_6]^{4-}$ octahedra that comprise the inorganic layers were evaluated using the following parameters:

Bond length distortion[5]: $\Delta_{oct}=\frac{1}{6}\sum_{i=1}^{6}\left[\frac{d_i-d_m}{d_m}\right]^2$ (1)

Octahedral elongation[6,7]: $\lambda_{oct}=\frac{1}{6}\sum_{i=1}^{6}\left[\frac{d_i}{d_0}\right]^2$ (2)

Octahedral angle variance[5-8]: $\sigma^2{}_{oct}=\frac{1}{11}\sum_{i=1}^{12}(\alpha_i-90)^2$ (3)

where d_i corresponds to Pb–Br bond length, d_m to average Pb-Br bond length, d_0 to the center-to-vertex distance of a regular octahedron of the same volume, and α_i to individual Br–Pb–Br angles. The parameters Δ_{oct}, λ_{oct} and $\sigma^2{}_{oct}$ provide a quantitative measure of octahedral distortion independent of the effective size of the octahedron. The crystallographic software VESTA was used in calculation of the structural distortion parameters λ_{oct} and $\sigma^2{}_{oct}$. The Pb-Br-Pb bond angles between conjoined $[PbBr_6]^{4-}$ octahedra were measured using the CCDC software Mercury.

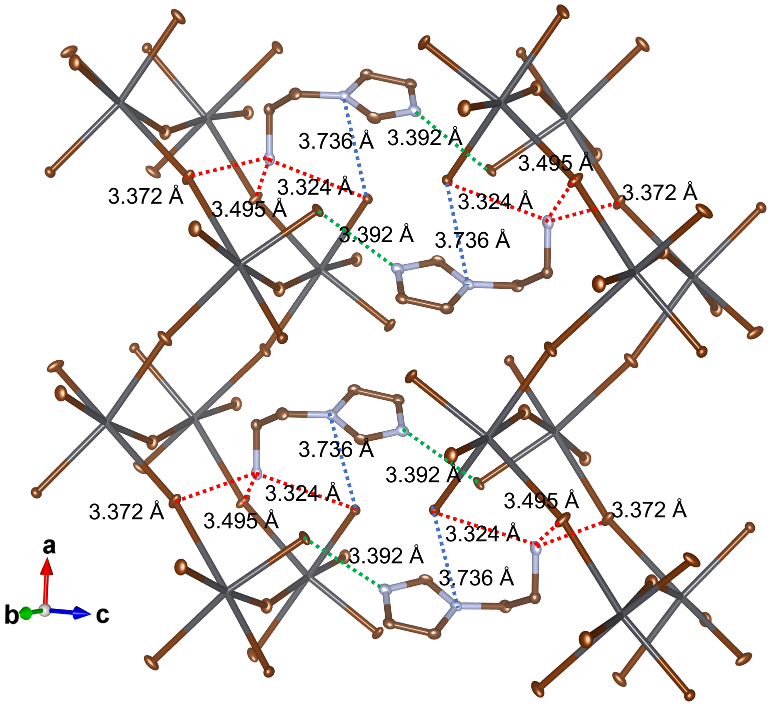

Figure S1. Crystal structure of **1**[PbBr$_4$] showing nearest neighbor contacts (Å) between the *N*-atoms of the dication **1**$^{2+}$ and the bridging or terminal Br$^-$ ions of the bromoplumbate lattice. Those involving the primary ammonium, endocyclic NH$^+$, and alkylated endocyclic *N*-atoms are depicted using red, green and blue dashed lines, respectively. Grey, brown, light brown and blue spheroids correspond to Pb, Br, C and N atoms, respectively. H atoms are omitted for clarity. Thermal ellipsoids are shown at 50% probability.

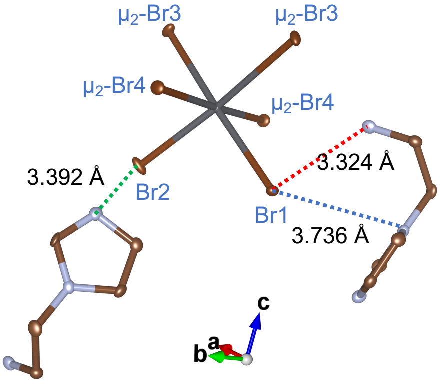

Figure S2. Shortest distances between the primary ammonium, endocyclic NH$^+$, and alkylated endocyclic *N*-atoms and terminal Br$^-$ ions of **2**[PbBr$_4$], depicted using red, green and blue dashed lines, respectively. These interactions promote formation of "cis" oriented terminal Br$^-$ in the inorganic lattice. Grey, brown, light brown and blue spheroids represent Pb, Br, C and N atoms, respectively. H atoms are omitted for clarity. Thermal ellipsoids are shown at 50% probability.

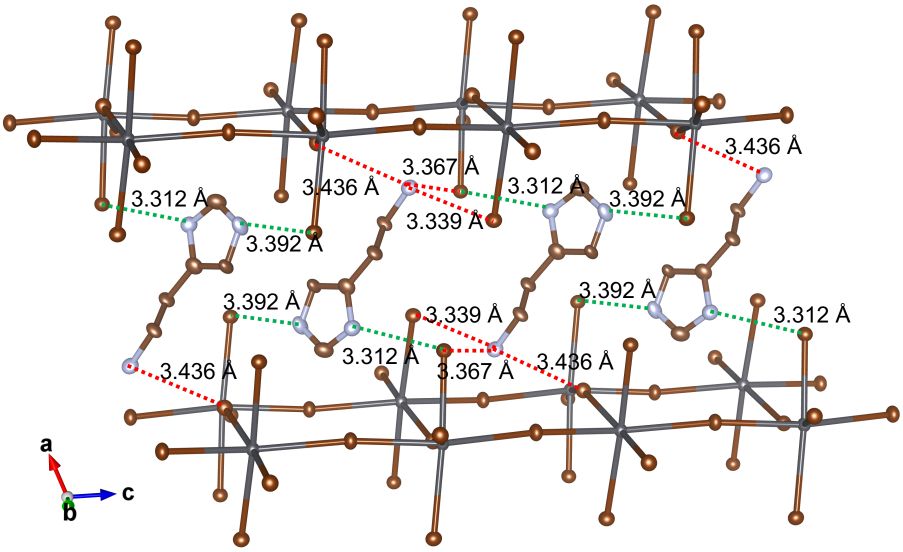

Figure S3. Crystal structure of **2**[PbBr4] showing nearest neighbor contacts (Å) between the *N*-atoms of the dication $\mathbf{2}^{2+}$ and the bridging or terminal Br^- ions of the (100)-oriented bromoplumbate lattice. Those involving the primary ammonium and endocyclic *N*-atoms are depicted using red and green dashed lines, respectively. Grey, brown, light brown and blue spheroids correspond to Pb, Br, C and N atoms, respectively. H atoms are omitted for clarity. Thermal ellipsoids are shown at 50% probability.

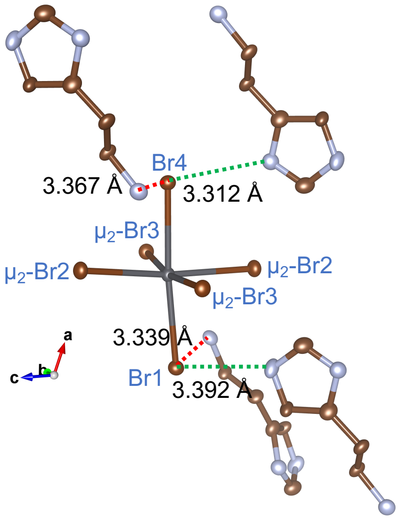

Figure S4. The shortest distances between the *N*-atoms of the primary ammonium group (red dashed line) and imidazolium ring (green dashed line) and terminal Br^- ions of **2**[PbBr4], which promote formation of "trans" oriented terminal Br^- ions in the inorganic lattice. Grey, brown, light brown and blue spheroids correspond to Pb, Br, C and N atoms, respectively. H atoms are omitted for clarity. Thermal ellipsoids are shown at 50% probability.

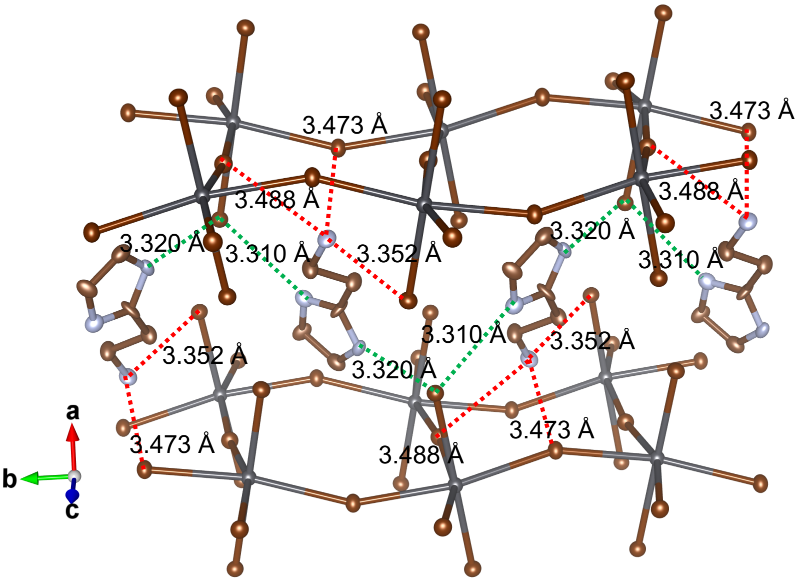

Figure S5. Crystal structure of **3**[$PbBr_4$] showing nearest neighbor contacts (Å) between the *N*-atoms of the dication $\mathbf{3}^{2+}$ and the bridging or terminal Br$^-$ ions of the (100)-oriented bromoplumbate lattice. Those involving the primary ammonium and endocyclic *N*-atoms are depicted using red and green dashed lines, respectively. Grey, brown, light brown and blue spheroids correspond to Pb, Br, C and N atoms, respectively. H atoms are omitted for clarity. Thermal ellipsoids are shown at 50% probability.

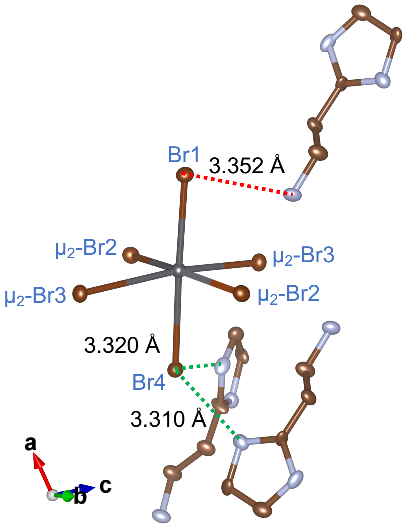

Figure S6. The shortest distances between the *N*-atoms of the primary ammonium group (red dashed line) and imidazolium ring (green dashed line) and terminal Br$^-$ ions of **3**[$PbBr_4$], which promote formation of "trans" oriented terminal Br$^-$ ions in the inorganic lattice. Grey, brown, light brown and blue spheroids correspond to Pb, Br, C and N atoms, respectively. H atoms are omitted for clarity. Thermal ellipsoids are shown at 50% probability.

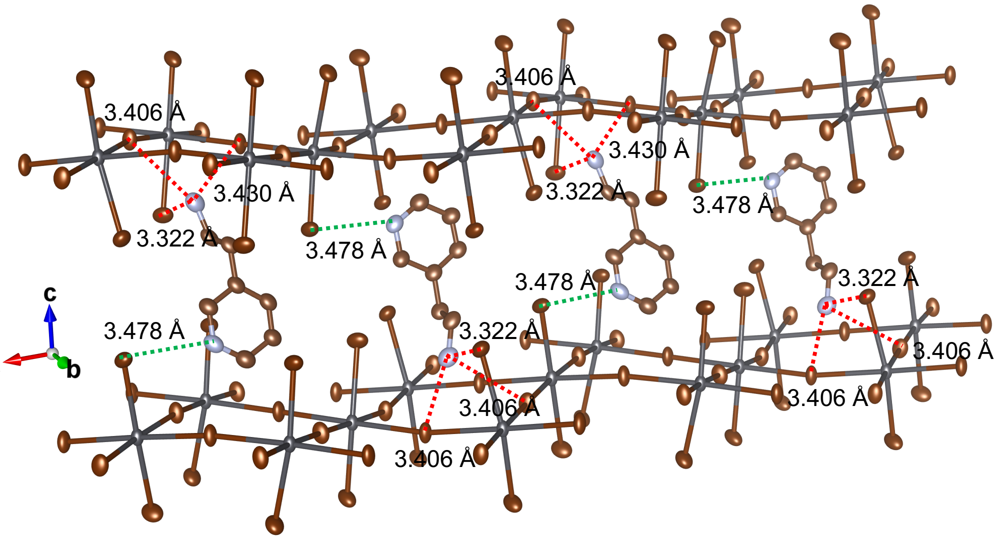

Figure S7. Crystal structure of **4**[PbBr$_4$] showing nearest neighbor contacts (Å) between the *N*-atoms of the dication **4**$^{2+}$ and the bridging or terminal Br$^-$ ions of the (100)-oriented bromoplumbate lattice. Those involving the primary ammonium and endocyclic *N*-atoms are depicted using red and green dashed lines, respectively. Grey, brown, light brown and blue spheroids correspond to Pb, Br, C and N atoms, respectively. H atoms are omitted for clarity. Thermal ellipsoids are shown at 50% probability.

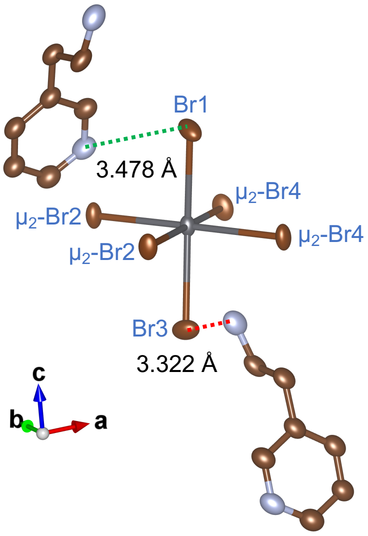

Figure S8. The shortest distances between the *N*-atoms of the primary ammonium group (red dashed line) and imidazolium ring (green dashed line) and terminal Br$^-$ ions of **4**[PbBr$_4$], which promote formation of "trans" oriented terminal Br$^-$ ions in the inorganic lattice. Grey, brown, light brown and blue spheroids correspond to Pb, Br, C and N atoms, respectively. H atoms are omitted for clarity. Thermal ellipsoids are shown at 50% probability.

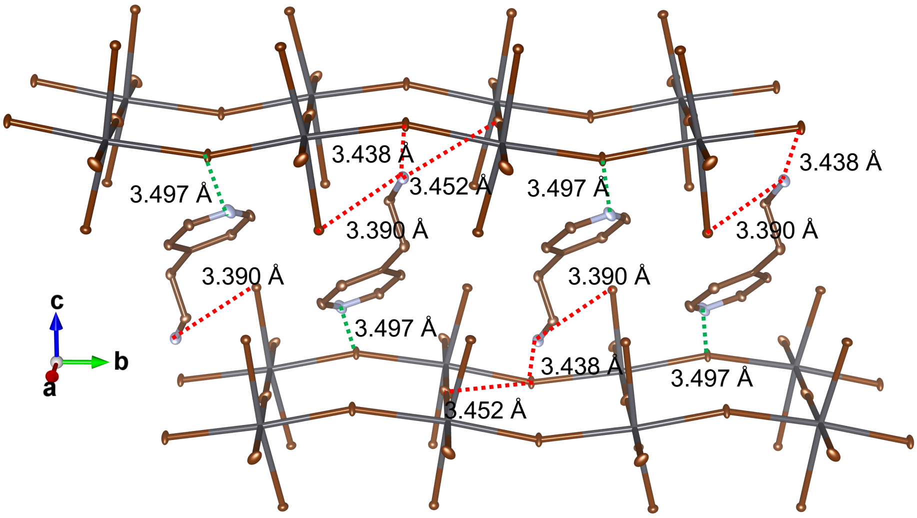

Figure S9. Crystal structure of **5**[PbBr$_4$] showing nearest neighbor contacts (Å) between the *N*-atoms of the dication $\mathbf{5}^{2+}$ and the bridging or terminal Br$^-$ ions of the (100)-oriented bromoplumbate lattice. Those involving the primary ammonium and endocyclic *N*-atoms are depicted using red and green dashed lines, respectively. Grey, brown, light brown and blue spheroids correspond to Pb, Br, C and N atoms, respectively. H atoms are omitted for clarity. Thermal ellipsoids are shown at 50% probability.

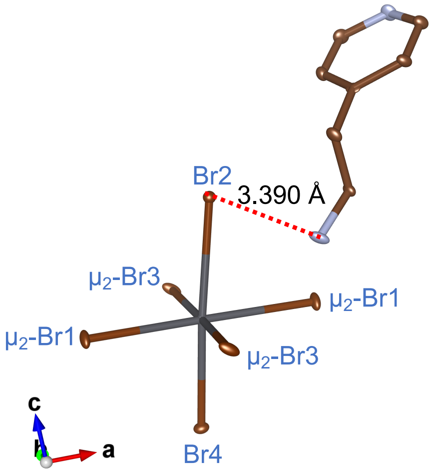

Figure S10. The shortest distances between the *N*-atoms of the primary ammonium group (red dashed line) and imidazolium ring (green dashed line) and terminal Br$^-$ ions of **5**[PbBr$_4$], which promote formation of "trans" oriented terminal Br$^-$ ions in the inorganic lattice. Grey, brown, light brown and blue spheroids correspond to Pb, Br, C and N atoms, respectively. H atoms are omitted for clarity. Thermal ellipsoids are shown at 50% probability.

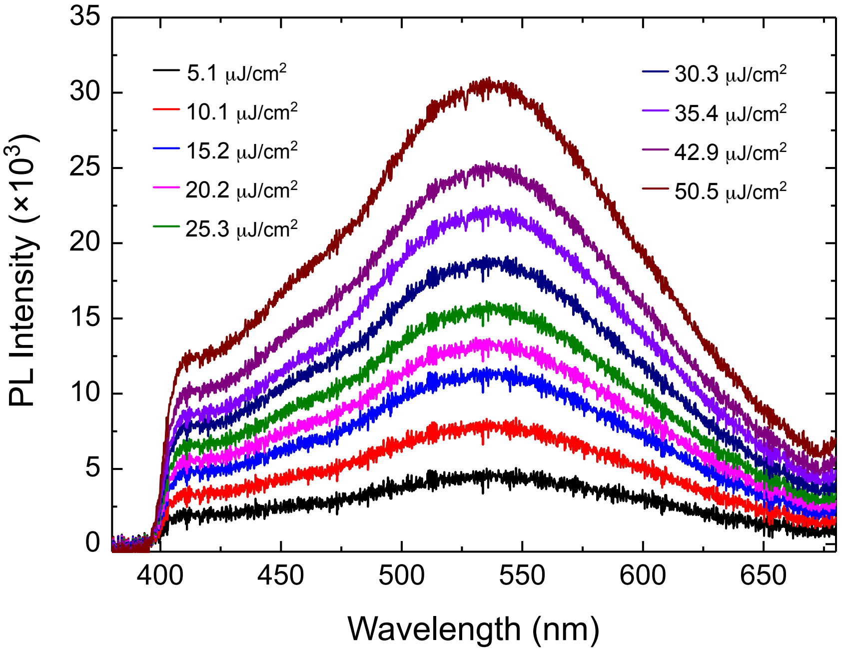

Figure S11. Evolution of the photoluminescence spectrum of **1**[PbBr$_4$] as a function of excitation fluence.

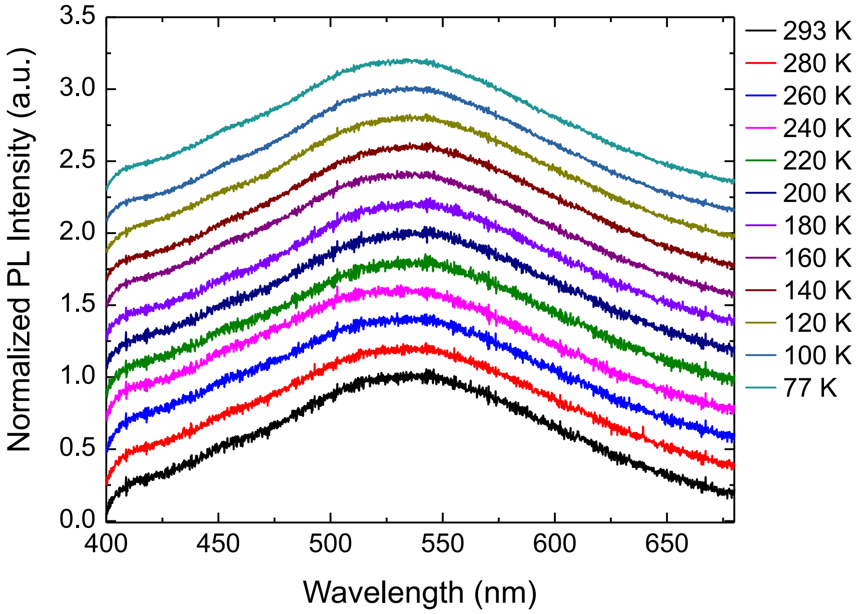

Figure S12. Evolution of the photoluminescence spectrum of **1**[PbBr$_4$] as a function of temperature.

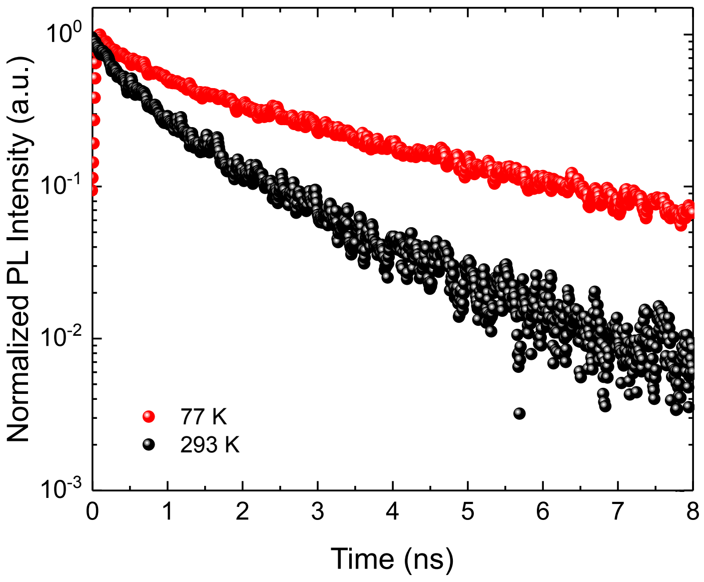

Figure S13. Time-resolved photoluminescence (PL) spectrum of **1**[PbBr$_4$], recorded at an emission wavelength of 550 nm, at temperatures of 293 and 77 K. Monoexponential fittings afforded PL lifetimes of *ca.* 1.43 and 3.31 ns at 293 and 77 K, respectively.

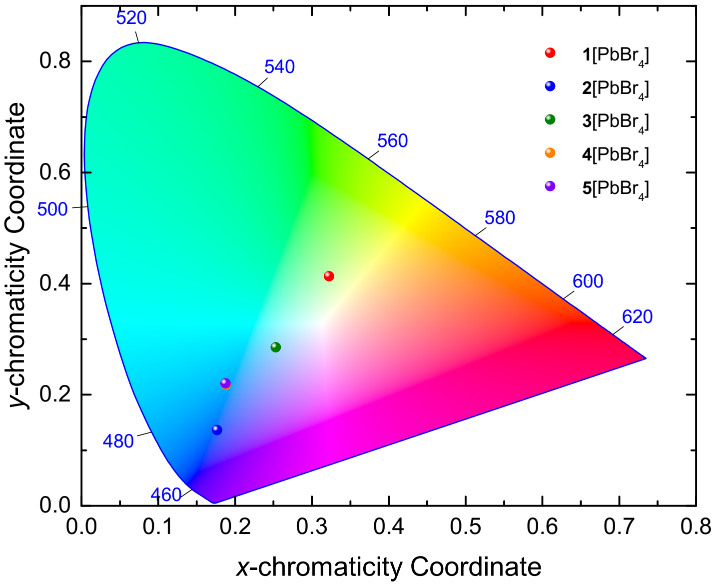

Figure S14. Chromaticity coordinates of emissions from compounds **1**[PbBr$_4$] – **5**[PbBr$_4$].

Table S1. Calculated intra-octahedral distortion parameters (Δ_{oct}) for **1**[PbBr$_4$] – **5**[PbBr$_4$].

Compound	Δ_{oct} (× 10^{-4})
1[PbBr$_4$]	22.93
2[PbBr$_4$]	5.82
3[PbBr$_4$]	11.37
4[PbBr$_4$]	2.63
5[PbBr$_4$]	4.73

Table S2. Comparison of the distortion parameters of **1**[PbBr$_4$] with previously reported 2 × 2 (110)-oriented 2D perovskites.

Compound	λ_{oct}[α]	σ^2_{oct}[b]	Δ_{oct} (×10^{-4})[c]
1[PbBr$_4$]	1.0177	53.67	22.93
ImPA[PbBr$_4$][d]	1.0088	20.80	26.02
IsEA[PbBr$_4$][e]	1.0123	38.89	9.67
N-MEDA[PbBr$_4$][f]	1.0080	24.51	8.20
EDBE[PbBr$_4$][g]	1.0090	23.91	24.00
EPZ[PbBr$_4$][h]	1.0164	40.26	38.07
3APr[PbBr$_4$][i]	1.0180	43.64	35.24

[α] Octahedral elongation. [b] Octahedral angle variance. [c] Octahedral bond-length distortion. [d] 1-(3-ammoniopropyl)-1H-imidazol-1-ium,[9] [e] Isothioureaethylammonium,[10] [f] *N*^{1}-methylethane-1,2-diammonium,[11] [g] 2,2′-(ethylenedioxy)bis(ethylammonium),[12] [h] 1-ethylpiperazinium,[13] [i] 3-aminopyrrolidinium.[14]

Table S3. Calculated Commission Internationale de l'Eclairage (CIE) chromaticity coordinates, Color Rendering Index (CRI), and Correlated Color Temperature (CCT) values for **1**[$PbBr_4$] – **5**[$PbBr_4$].

Compound	CIE x-coordinate	CIE y-coordinate	CRI	CCT
1[$PbBr_4$]	0.3223	0.4131	73	5824
2[$PbBr_4$]	0.1765	0.1363	46	-
3[$PbBr_4$]	0.2532	0.2853	85	14223
4[$PbBr_4$]	0.1879	0.2177	57	-
5[$PbBr_4$]	0.1875	0.2201	56	-

Table S4. Crystallographic and structure refinement data for **1**[$PbBr_4$] – **5**[$PbBr_4$].$^{\alpha}$

	Compound				
	1[$PbBr_4$]	**2**[$PbBr_4$]	**3**[$PbBr_4$]	**4**[$PbBr_4$]	**5**[$PbBr_4$]
Empirical formula	$C_5H_{10}Br_4N_3Pb$	$C_5H_5Br_4N_3Pb$	$C_5H_{10}Br_4N_3Pb$	$C_7H_{12}Br_4N_2Pb$	$C_7H_{12}Br_4N_2Pb$
Formula weight	638.99 g/mol	633.95 g/mol	638.99 g/mol	651.02 g/mol	651.02 g/mol
Temperature	100(2) K	100(2) K	100(2) K	100(2) K	100(2) K
Wavelength	0.71073 Å	0.71073 Å	0.71073 Å	0.71073 Å	0.71073 Å
Crystal size	0.080 x 0.100 x 0.120 mm	0.020 x 0.040 x 0.120 mm	0.020 x 0.060 x 0.200 mm	0.020 x 0.040 x 0.220 mm	0.040 x 0.080 x 0.120 mm
Crystal habit	colorless block	colorless plate	colorless plate	yellow needle	yellow plate
Crystal system	orthorhombic	monoclinic	monoclinic	orthorhombic	monoclinic
Space group	P b c a	P 1 21/c 1	P 1 21/c 1	P b c a	P 1 21/n 1
Unit cell dimensions	a = 9.5053(2) Å	a = 10.5249(7) Å	a = 10.0629(6) Å	a = 16.8270(7) Å	a = 5.9837(2) Å
	α = 90°	α = 90°	α = 90°	α = 90°	α = 90°
	b = 11.7946(2) Å	b = 11.4885(7) Å	b = 11.6838(8) Å	b = 8.3941(3) Å	b = 11.8526(4) Å
	β = 90°	β = 109.985(2)°	β = 108.486(4)°	β = 90°	β = 93.9990(14)°
	c = 23.5189(4) Å	c = 11.9069(7) Å	c = 11.9306(10) Å	c = 19.8920(9) Å	c = 19.4795(6) Å
	γ = 90°	γ = 90°	γ = 90°	γ = 90°	γ = 90°
Volume	2636.73(8) Å^3	1353.03(15) Å^3	1330.34(17) Å^3	2809.7(2) Å^3	1378.17(8) Å^3
Z	8	4	4	8	4
Density	3.219 g/cm^3	3.112 g/cm^3	3.190 g/cm3	3.078 g/cm^3	3.138 g/cm^3
Absorption coefficient	24.886 mm^{-1}	24.248 mm^{-1}	24.662 mm^{-1}	23.355 mm^{-1}	23.808 mm^{-1}
F(000)	2264	1112	1132	2320	1160
Theta range for data collection	2.88 to 31.00°	2.54 to 30.00°	2.51 to 31.04°	2.38 to 27.00°	2.71 to 34.00°
Reflections collected	30720	15540	4187	18962	24583

Coverage of independent reflections	99.9%	99.9%	99.3%	100.00%	99.90%
Absorption correction	Multi-Scan	Multi-Scan	Multi-Scan	Multi-Scan	Multi-Scan
Max. and min. transmission	0.2410 and 0.1540	0.6430 and 0.1590	0.6380 and 0.0830	0.6520 and 0.0790	0.4490 and 0.1620
Function minimized	Σ w(F_o^2 - F_c^2)^2	Σ w(F_o^2 - F_c^2)^2	Σ w(F_o^2 - F_c^2)^2	Σ w(F_o^2 - F_c^2)^2	Σ w(F_o^2 - F_c^2)^2
Data / restraints / parameters	4193 / 0 / 119	3944 / 0 / 119	4187 / 0 / 120	3065 / 411 / 211	5625 / 0 / 128
Goodness-of-fit on F^2	1.069	1.036	1.042	1.058	1.027
Δ/σmax	0.001	0.001	0.001	0.001	0.001
Final *R* indices [I > 2σ(I)]	3378 data R1 = 0.0251, wR2 = 0.0430	2902 data R1 = 0.0451, wR2 = 0.0902	2941 data R1 = 0.0650, wR2 = 0.1279	2253 data R1 = 0.0433, wR2 = 0.0937	4466 data R1 = 0.0328, wR2 = 0.0580
R indices [all data]	R1 = 0.0396, wR2 = 0.0471	R1 = 0.0708, wR2 = 0.1018	R1 = 0.1061, wR2 = 0.1503	R1 = 0.0676, wR2 = 0.1089	R1 = 0.0503, wR2 = 0.0637
Largest diff. peak and hole	1.060 and -1.188 eÅ^{-3}	2.091 and -1.623 eÅ^{-3}	3.031 and -2.676 eÅ^{-3}	2.133 and -1.832 eÅ^{-3}	1.289 and -2.076 eÅ^{-3}
R.M.S. deviation from mean	0.263 eÅ^{-3}	0.301 eÅ^{-3}	0.491 eÅ^{-3}	0.254 eÅ^{-3}	0.339 eÅ^{-3}

$^{\alpha}R = \Sigma||F_o| - |F_c||/\Sigma|F_o|$, w$R = \{\Sigma[w(|F_o|^2 - |F_c|^2)^2]/\Sigma[w(|F_o|^4)]\}^{1/2}$ and **1**[PbBr$_4$], $w = 1/[\sigma^2(F_o^2) + (0.0150P)^2 + 0.2316P]$; **2**[PbBr$_4$], $w = 1/[\sigma^2(F_o^2) + (0.0298P)^2 + 3.1350P]$; (**3**[PbBr$_4$], $w = 1/[\sigma^2(F_o^2) + (0.0472P)^2 + 21.4593P]$; **4**[PbBr$_4$], $w = 1/[\sigma^2(F_o^2) + (0.0346P)^2 + 42.7986P]$; **5**[PbBr$_4$], $w = 1/[\sigma^2(F_o^2) + (0.0167P)^2]$; where $P = (F_o^2+2F_c^2)/3$.

Table S5. Pb-Br bond lengths in **1**[$PbBr_4$].

Bonds	Distances (Å)
Br1-Pb1	2.9082(4)
Br3-Pb1	3.1177(4)
Br4-Pb1	3.0242(4)
Br2-Pb1	2.7735(4)
Br3-Pb1	3.2260(4)
Br4-Pb1	3.0272(4)

Table S6. Selected bond angles in **1**[$PbBr_4$].

Bonds	Angles (°)	Bonds	Angles (°)
Pb1-Br3-Pb1	168.381(16)	Br2-Pb1-Br1	91.235(13)
Br2-Pb1-Br4	83.445(13)	Br1-Pb1-Br4	98.038(13)
Br2-Pb1-Br4	94.895(13)	Br1-Pb1-Br4	87.167(12)
Br4-Pb1-Br4	174.556(8)	Br2-Pb1-Br3	87.439(13)
Br1-Pb1-Br3	165.010(13)	Br4-Pb1-Br3	96.643(13)
Br4-Pb1-Br3	78.080(12)	Br2-Pb1-Br3	164.355(13)
Br1-Pb1-Br3	87.324(11)	Br4-Pb1-Br3	81.338(12)
Br4-Pb1-Br3	100.587(12)	Br3-Pb1-Br3	97.885(4)
Pb1-Br4-Pb1	154.573(17)		

Table S7. Pb-Br bond lengths in **2**[$PbBr_4$].

Bonds	Distances (Å)
Pb1-Br2	2.9026(10)
Pb1-Br4	2.9371(9)
Pb1-Br3	3.0513(10)
Pb1-Br3	2.9140(10)
Pb1-Br1	3.0212(10)
Pb1-Br2	3.0917(10)

Table S8. Selected bond angles in **2**[$PbBr_4$].

Bonds	Angles (°)	Bonds	Angles (°)
Br2-Pb1-Br3	87.04(3)	Br2-Pb1-Br4	89.55(3)
Br3-Pb1-Br4	88.38(3)	Br2-Pb1-Br1	86.57(3)
Br3-Pb1-Br1	88.50(3)	Br4-Pb1-Br1	175.14(3)
Br2-Pb1-Br3	85.70(3)	Br3-Pb1-Br3	170.747(16)
Br4-Pb1-Br3	85.84(3)	Br1-Pb1-Br3	96.77(3)
Br2-Pb1-Br2	166.94(2)	Br3-Pb1-Br2	82.55(3)
Br4-Pb1-Br2	82.33(3)	Br1-Pb1-Br2	100.95(3)
Br3-Pb1-Br2	103.79(3)	Pb1-Br3-Pb1	150.29(4)
Pb1-Br2-Pb1	173.17(4)		

Table S9. Pb-Br bond lengths in **3**[$PbBr_4$].

Bonds	Distances (Å)
Br1-Pb1	2.9312(14)
Br2-Pb1	3.0515(15)
Br3-Pb1	3.1748(17)
Br2-Pb1	2.9446(15)
Br3-Pb1	2.8684(17)
Br4-Pb1	3.0566(15)

Table S10. Selected bond angles in **3**[$PbBr_4$].

Bonds	Angles (°)	Bonds	Angles (°)
Pb1-Br2-Pb1	156.39(6)	Br3-Pb1-Br1	87.98(5)
Br3-Pb1-Br2	86.29(5)	Br1-Pb1-Br2	92.21(4)
Br3-Pb1-Br2	84.44(5)	Br1-Pb1-Br2	92.70(4)
Br2-Pb1-Br2	169.35(2)	Br3-Pb1-Br4	89.77(4)
Br1-Pb1-Br4	177.74(5)	Br2-Pb1-Br4	87.43(4)
Br2-Pb1-Br4	87.30(4)	Br3-Pb1-Br3	162.28(3)
Br1-Pb1-Br3	103.00(5)	Br2-Pb1-Br3	79.50(4)
Br2-Pb1-Br3	108.53(4)	Br4-Pb1-Br3	79.13(4)
Pb1-Br3-Pb1	170.35(5)		

Table S11. Pb-Br bond lengths in **4**[$PbBr_4$].

Bonds	Distances (Å)
Br1-Pb1	2.9086(14)
Br2-Pb1	2.9934(11)
Br4-Pb1	2.9837(12)
Br2-Pb1	2.9796(11)
Br3-Pb1	3.0760(14)
Br4-Pb1	2.9872(12)

Table S12. Selected bond angles in **4**[$PbBr_4$].

Bonds	Angles (°)	Bonds	Angles (°)
Pb1-Br2-Pb1	168.95(5)	Pb1-Br4-Pb1	178.64(5)
Br1-Pb1-Br2	90.61(4)	Br1-Pb1-Br4	92.01(4)
Br2-Pb1-Br4	87.99(4)	Br1-Pb1-Br4	90.55(4)
Br2-Pb1-Br4	177.11(4)	Br4-Pb1-Br4	89.329(11)
Br1-Pb1-Br2	89.70(4)	Br2-Pb1-Br2	89.486(12)
Br4-Pb1-Br2	176.97(4)	Br4-Pb1-Br2	93.16(4)
Br1-Pb1-Br3	169.83(5)	Br2-Pb1-Br3	93.59(4)
Br4-Pb1-Br3	97.39(4)	Br4-Pb1-Br3	85.70(4)
Br2-Pb1-Br3	81.09(4)		

Table S13. Pb-Br bond lengths in **5**[$PbBr_4$].

Bonds	Distances (Å)
Br1-Pb1	2.9794(4)
Br2-Pb1	3.0723(5)
Br3-Pb1	3.0687(5)
Br1-Pb1	3.0045(4)
Br3-Pb1	2.9579(5)
Br4-Pb1	2.8841(5)

Table S14. Selected bond angles in **5**[$PbBr_4$].

Bonds	Angles (°)	Bonds	Angles (°)
Pb1-Br1-Pb1	179.13(2)	Pb1-Br3-Pb1	159.475(17)
Br4-Pb1-Br3	87.752(14)	Br4-Pb1-Br1	94.466(13)
Br3-Pb1-Br1	90.254(15)	Br4-Pb1-Br1	85.247(13)
Br3-Pb1-Br1	90.554(14)	Br1-Pb1-Br1	179.13(2)
Br4-Pb1-Br3	94.807(14)	Br3-Pb1-Br3	175.732(6)
Br1-Pb1-Br3	92.946(14)	Br1-Pb1-Br3	86.262(14)
Br4-Pb1-Br2	172.269(14)	Br3-Pb1-Br2	86.276(13)
Br1-Pb1-Br2	80.666(12)	Br1-Pb1-Br2	99.706(12)
Br3-Pb1-Br2	91.455(13)		

References:

1. SAINT and SADABS; Bruker AXS Inc.: Madison, WI, (2007).
2. Sheldrick, G. M. *SHELXL-97*, *Program for crystal structure refinement*; Göttingen, **1997**.
3. G. M. Sheldrick, *Acta Crystallogr., Sect. A: Found. Crystallogr.,* 2008, **64**, 112–122.
4. K. Momma and F. Izumi, *Commission on Crystallogr. Comput.,* 2006, **7**, 106–119.
5. A. Ertl, J. M. Hughes, F. Pertlik, F. F. F. Jr., S. E. Wright, F. Brandstatter and B. Marler, *Can. Mineral.,* 2002, **40**, 153–162.
6. K. Robinson, G. V. Gibbs and P. H. Ribbe, *Science* 1971, **172**, 567–570.
7. N. W. Thomas, *Acta Crystallographica Section B* 1989, **45**, 337–344.
8. M. E. Fleet, *Mineralogical Magazine* 1976, **40**, 531–533.
9. Y. Y. Li, C. K. Lin, G. L. Zheng, Z. Y. Cheng, H. You, W. D. Wang, and J. Lin, *Chem. Mater.*, 2006, **18**, 3463–3469.
10. Y. Li, G. Zheng and J. Lin, *Eur. J. Inorg. Chem.*, 2008, **2008**, 1689–1692.
11. E. R. Dohner, E. T. Hoke and H. I. Karunadasa, *J. Am. Chem. Soc.*, 2014, **136**, 1718–1721.
12. E. R. Dohner, A. Jaffe, L. R. Bradshaw and H. I. Karunadasa, *J. Am. Chem. Soc.*, 2014, **136**, 13154–13157.
13. L. Mao, P. Guo, M. Kepenekian, I. Hadar, C. Katan, J. Even, R. D. Schaller, C. C. Stoumpos and M. G. Kanatzidis, *J. Am. Chem. Soc.*, 2018, **140**, 13078–13088.
14. X. Li, P. Guo, M. Kepenekian, I. Hadar, C. Katan, J. Even, C. C. Stoumpos, R. D. Schaller, and M. G. Kanatzidis, *Chem. Mater.,* 2019, **31**, 3582−3590.